Steel and Composite Structures, *Vol. 31*, *No. 1* (*2019*) *69-83*
DOI: https://doi.org/10.12989/scs.2019.31.1.069

Experimental behavior of VHSC encased composite stub column under compression and end moment

Zhenyu Huang [1,2], Xinxiong Huang [1,2a], Weiwen Li [*1,2], Liu Mei [**1,2] and J.Y. Richard Liew [3b]

[1] *Guangdong Provincial Key Laboratory of Durability of Marine Civil Engineering*, *Shenzhen University*, *Shenzhen 518060*, *China*
[2] *College of Civil Engineering*, *Shenzhen University*, *Shenzhen 518060*, *China*
[3] *Department of Civil and Environmental Engineering*, *National University of Singapore*, *Blk E1A*,*#07-03*, *1 Engineering Drive 2*, *Singapore 117576*, *Singapore*

(*Received December 9*, *2018*, *Revised March 14*, *2019*, *Accepted March 19*, *2019*)

Abstract. This paper investigates the structural behavior of very high strength concrete encased steel composite columns via combined experimental and analytical study. The experimental programme examines stub composite columns under pure compression and eccentric compression. The experimental results show that the high strength encased concrete composite column exhibits brittle post peak behavior and low ductility but has acceptable compressive resistance. The high strength concrete encased composite column subjected to early spalling and initial flexural cracking due to its brittle nature that may degrade the stiffness and ultimate resistance. The analytical study compares the current code methods (ACI 318, Eurocode 4, AISC 360 and Chinese JGJ 138) in predicting the compressive resistance of the high strength concrete encased composite columns to verify the accuracy. The plastic design resistance may not be fully achieved. A database including the concrete encased composite column under concentered and eccentric compression is established to verify the predictions using the proposed elastic, elastoplastic and plastic methods. Image-oriented intelligent recognition tool-based fiber element method is programmed to predict the load resistances. It is found that the plastic method can give an accurate prediction of the load resistance for the encased composite column using normal strength concrete (20-60 MPa) while the elastoplastic method provides reasonably conservative predictions for the encased composite column using high strength concrete (60-120 MPa).

Keywords: composite column; concrete encased column; high strength concrete; steel-concrete composite; ultra-high strength concrete

1. Introduction

Structural concrete can be classified as conventional concrete, high strength, very high strength concrete and ultra-high strength concrete as listed in Table 1 (Kim *et al*. 2017a). The development of high strength concrete is a major progress in concrete technology due to its superior advantages such as high strength, high abrasion, low permeability and facilitating the design of smaller structural sections to meet the architectural and economic requirements. Such advantages enable a wide range of potential engineering application of high strength concrete on high rise buildings, long-span bridges, blast resistant structures, nuclear power plant structures and offshore infrastructures (Huang *et al*. 2015, Huang and Liew 2016a).

Extensive researchers have attempted to investigate the mechanical behavior of high strength concrete. Some focus on the effect of coarse aggregate types (Lee 2013), curing conditions, shrinkage and creep, flexural behavior (Bărbos 2016) and the effect of high temperature exposures (Choe *et al*. 2015, Xiong and Liew 2016) and the confined behavior of high strength (Zohrevand and Mirmiran 2013, Deng and Qu 2015). However, there are quite few investigations on the structural behavior of high strength concrete encased composite column (Kim *et al*. 2012, 2014, Zhu *et al*. 2017). Concrete encased composite column is a section in which the steel is fully or partially covered by concrete where the three components work together to provide higher load resistance (El-Tawil and Deierlein 1999, Pereira *et al*. 2016, Elwi *et al*. 2015). There two typical types of concrete encased composite column, namely, partially and fully encased sections (Eurocode 4 2004). The use of encased section reduces the volume to strength ratio and provides superior fire resistance as well as the prevention of local buckling of steel section as compared to the concrete filled-tube (CFT) composite columns. Concrete encased composite column is more effective construction member with very high compressive resistance, good ductility if properly reinforced by steel and is more durable with very low permeability coefficient compared to the conventional reinforced concrete columns (Lu *et al*. 2014, Yang *et al*. 2018). There are some current available design codes for concrete encased column design practice such as AIJ (2010), AISC 360 (2010), Eurocode 4 (2004), YB 9082

*Corresponding author, Ph.D., Professor,
E-mail: liweiwen@szu.edu.cn
**Co-corresponding author, Ph.D., Lecturer,
E-mail: mayleeu@126.com
[a] Master Student
[b] Professor

ISSN: 1229-9367 (Print), 1598-6233 (Online)

Table 1 Concrete classification

Items	CC	HSC	VHSC	UHSC
Strength (MPa)	< 50	50-100	100-150	> 150
Water-cement ratio	> 0.45	0.45-0.3	0.3-0.25	< 0.25
Chemical admixtures	No	WRA/HRWR*	HRWR	HRWR
Mineral admixtures	No	Fly ash	Silica fume	Silica fume
Permeability coefficient (cm/s)	$> 10^{-10}$	10^{-11}	10^{-12}	$< 10^{-13}$

*CC = conventional concrete; HSC = high strength concrete; VHSC = very high strength concrete; UHSC = ultra-high strength concrete; WRA = water reducing admixture; HRWR = high-range water reducer

(2007) and JGJ 138 (2016). However, there is no unified design theory among these codes and the current codes basically are limited for composite columns using normal strength concrete (e.g., compressive strength of 20-90 MPa). Table 2 lists the strength grades of structural steel and concrete used in abovementioned design codes, showing that the steel grades are not higher than 525 MPa while the concrete strength is not higher than 90 MPa. As the development of high-performance concrete and structural steel, an increasingly number of civil structures utilize high strength high performance materials. High performance concrete may use less cement and water to reduce the carbon dioxide emission therefore mitigating the greenhouse effect. High performance concrete may require sufficient industry wastes like fly ash from coal-burning power plant, granulated ground blast furnace slag (GGBS) from steel production factory. In this case, the industrial waste can be properly disposed and utilized, which will form virtuous production-consumption cycle chain and lead to reduce carbon dioxide footprints. However, very high strength concrete is a new class of concrete that may not be covered in composite column design codes. VHSC exhibits brittle behavior such that it may greatly influence the failure mechanism, ductility and energy dissipation behavior of composite columns. Therefore, it is quite essential to assess the structural performance of VHSC encased composite column.

Table 2 Range of material strength utilized in design codes

Design code	f_y (MPa)	f_{ck} (MPa)
AISC 360	<= 525	21-70
Eurocode 2/4	<= 355	20-90
AIJ-SRC 2001	<= 440	18-90
YB 9082-2006	<= 345	30-80
JGJ 138-2016	<= 345	30-60

Kim *et al*. (2012, 2014, 2017a, b) investigated the compressive behavior of concrete encased composite column and concrete filled steel tube composite columns using ultra high strength concrete under eccentric loads, which are valuable results to the practice. Composite columns with good confinement by using the tie bar restraints exhibited ductile behavior, maintaining their high strength even after crushing of concrete. However, the peak load resistance was not greater than the initial crushing load because the strain of the steel section was not fully developed. Ellobody *et al*. (2011) investigated eccentrically loaded concrete encased composite column with varying the concrete strength from 30 to 110 MPa and the steel yield strength from 275 to 690 MPa numerically. It was found that EC4 accurately predicted the axial resistance of eccentrically loaded composite columns while overestimated the moment resistance. Later on, they (Ellobody and Young 2011) conducted more numerical studies including the slender column, non-slender column, stub and long columns using the normal and high strength concrete or steel. The comprehensive studies provided promising benchmark numerical modelling for high strength concrete encased composite columns. They also commented that it may not be easy to correctly simulate the high nonlinearity portion of the load–displacement curve by FEM. The using of new materials would lead to unknown failure modes. The comparison of the ultimate resistance between FE and tests may not be sufficient. Therefore, the insufficient testing data and lack of evaluation on the performance of high strength concrete encased composite columns indicates a need of research in this area.

This paper aims to promote the use of advanced high strength concrete in precast module building construction which are specifically to: (1) Develop an economical and practical very high strength concrete (VHSC) mix(es) that has a target compressive strength of at least 100 MPa and performance characteristics superior to normal concrete; (2) Investigate the use of the developed VHSC mixes in precast concrete encased composite columns and examine the failure mechanism; (3) Evaluate the experimental behavior of VHSC encased composite columns subjected to both axial compression and uniaxial end moment and to derive a method to predict the combined compression and moment resistance; (4) Verify the current design methods through a series of compressive tests and a four point bending test. Structural behavior of both steel fiber reinforced and conventional reinforced concrete columns are also discussed. Improved elastic, elastoplastic and plastic approaches are proposed to predict the resistance of VHSC encased composite columns. This paper also establishes a database of experimental results of concrete encased composite columns subjected to eccentric loading from the literature (Ye 1995, Lou 1996, Gentian *et al*. 2006, Lin 2006, Wang 2007, Zhang 2011, Kim *et al*. 2012, 2014, Begum *et al*. 2013). To come up with a design guide, the proposed design methods were also validated against the test data.

Table 3 Mix proportions of VHSC

Mix ID	W/B	OPC	SF	SL	FAgg	CAgg	SRA	HWRA
VHSC-#1	0.18	700	100	200	1250	-	10	10
VHSC-#2	0.18	700	100	200	500	750	10	10
VHSC-#3	0.18	700	100	200	1250	-	-	20

*W/B = water to binder ratio; OPC = ordinary Portland cement; SF = silica fume; SL = slag; FAgg = fine aggregates; CAgg = coarse aggregates; SRA = shrinkage reducing agent; HWRA = high water reducing agent

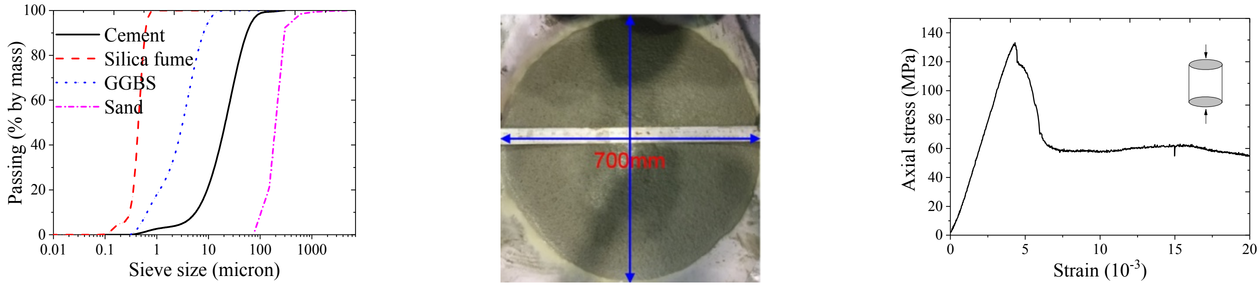

(a) Particle size distributions of cement, silica fume, GGBS and sand

(b) Slump flow test of VHSC

(c) Stress-strain curve of VHSC under axial compression

Fig. 1 Properties of raw materials and VHSC

Table 4 Material properties of concrete samples

Concrete type	Specimen	f_{ck} (MPa)	f_c (MPa)	E_c (GPa)	v_c
NWC	C50	51.1	49.8	37.3	
VHSC	C100	109.3	109.0	44.9	0.25
	C100F	123.8	130.4	47.6	

* NWC = normal weight concrete; f_{ck} = cylinder compressive strength; f_c = cube compressive strength; E_c = Young's modulus (secant modulus E_c defined at $0.45f_c$' according to ACI 318, v_c = Poisson ratio

2. Experimental program

2.1 Material properties

To prepare concrete encased composite columns, three types of concretes, namely, normal concrete, Very High Strength Concrete (VHSC) with and without steel fibers were considered. The concrete was designed to have a target 28-day cylinder compressive strength around 50 MPa (C50) and 100 MPa (C100), respectively. Table 3 shows the mixture proportions of VHSC. The VHSC matrix had a water-to-binder ratio of below 0.18 to achieve high strength. The binder consisted of 70wt% of CEM I 52.5R ordinary Portland cement and 10wt% of silica fume (Elkem Microsilica Grade 940 U) and 20 wt% of granulated ground blast furnace slag (GGBS). Silica fume was used to strengthen the bond resistance of interface transition zone between the cement paste and aggregates. The filler comprised 100wt% of finely graded sand or 40wt% sand and 60wt% of coarse aggregates. Finely graded sand and coarse aggregates were based on ASTM C136 (2014) which aimed to increase the packing density and thus improved the rheological properties of fresh paste. Fig. 1(a) shows the particle size distributions of raw materials. A polycarboxylate-based superplasticizer (SP) with 30% solid content by mass was used to reach desired workability. Before casting, the slump flow value of all the mixtures was measured based on ASTM C1611 (2018) as shown in Fig. 1(b). The specimens were demoulded after 24 h curing at room temperature and were cured with the column specimens until the test day. Fig. 1(c) shows the typical compressive stress-strain curve of VHSC. Three Φ100×200 mm concrete cylinders and three 100×100×100 mm concrete cubes were tested for each mixture, according to ASTM C39/C39M-01 (2014). Table 4 shows the mechanical properties of hardened VHSC an normal weight concrete used in the test.

Mild steel S355, HRB 335 rebar and HPB 300 stirrup were used for column fabrication. According to ASTM E8/E8M-16 (2016), direct tension tests on steel/rebar coupons using a universal test machine under displacement control were performed. The Young's modulus Es, Poisson ratio υ_s, 0.2% offset yield strength f_y of steel plate, rebar and stirrup are listed in Table 5.

Table 5 Material properties of steel plate, rebar and stirrup

Item	Component	E_s (MPa)	f_y (MPa)	υ_s
Steel flange	Mile steel	201.6	362.9	
Steel web	Mile steel	187.4	363.6	0.3
Rebar	HRB 400Φ16	193.6	356.8	
Stirrup	HPB 400Φ6	225.1	339.4	

* f_y = yield strength of steel; E_s = Young's modulus of steel; υ_s = Poisson ratio of steel

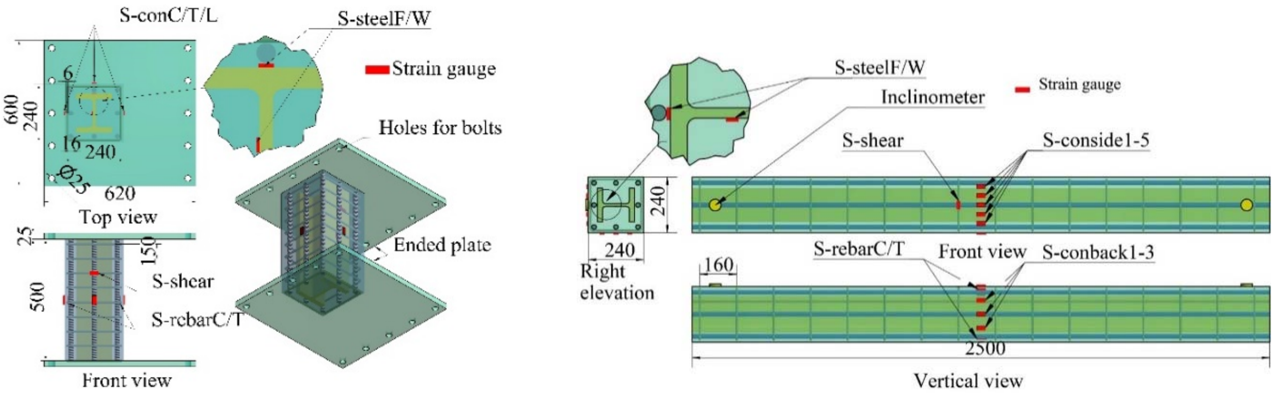

(a) Dimensions and strain gauges layout for short columns

(b) Dimensions and strain gauges layout for long column for four-point bending

Fig. 2 Dimensions and strain gauges layout of specimens

Table 6 Dimension of test specimens

NO.	Specimen	B(mm)	H(mm)	f_c (MPa)	f_y (MPa)	f_s (MPa)	e (mm)	Steel section
1	C50e0	240	240	51.1	363.3	356.8	0	UC152X152X37
2	C100e0	240	240	109.3	363.3	356.8	0	
3	C100e50	240	240	109.3	363.3	356.8	50	
4	C100e105	240	240	109.3	363.3	356.8	105	
5	C100B	240	240	109.3	363.3	356.8	-	
6	C100Fe0	240	240	123.8	363.3	-	0	

*B = width of specimen; H = height of specimen; f_c = strength of concrete; f_y = strength of steel face plate; f_s = strength of reinforcement rebars; e = loading eccentricity; Steel section = dimensions of steel plate

2.2 Design consideration

A total of six full-scaled VHSC encased composite column specimens were prepared, among which three specimens were under pure compression, one subjected to pure bending and two subjected to combine compression and bending by changing loading eccentricity e, respectively. The composite column consisted of a S355 steel section UC152X152X37 and was encased with normal concrete (C50e0), VHSC (C100e0, C100e50, C100e105, C100B) and fibre reinforced high strength concrete (C100Fe0,) respectively. As shown in Fig. 2(a), the short columns were designed to avoid global buckling with an overall height of 500 mm. The relative slenderness ratio λ = 0.14 < 2.0 according to Eurocode 4. In the test, a square size of 240×240 mm was selected. Two cover plates were welded on both ends of the specimens in order to be loaded uniformly. Stiffeners were provided to enhance both ends of the composite column to ensure that premature failure would not occur within the end region. The columns (shown as Fig. 2(b)) for four-point bending test were designed to be as long as 2500 mm in order to capture the flexural resistance, while other geometrical conditions and material properties kept the same. The ratio of steel section area to the gross section area was 8.18%. The steel contribution ratio satisfied the restriction of $0.2 < \delta < 0.9$, according to Eurocode 4. Eight rebars with a diameter of 16 mm were employed as longitudinal reinforcement. The rebar reinforcement ratio was 1.54%, satisfying the restriction of 0.3%-6% based on Eurocode 4. According to Eurocode 2 (2004), the minimum diameter of shear stirrups was required to not less than 6 mm and 0.25D (D is the diameter of longitudinal rebar), and the maximum spacing of stirrups was limited to the smallest value of 20 times diameter of longitudinal rebar, 400 mm and the smallest dimension of steel section. Therefore, the spacing of 150 mm with a stirrup diameter of 6 mm was employed in the test. The detailed information of the specimens is listed in Table 6.

2.3 Test set-up, loading procedure and instrumentations

Fig. 3 shows the test set-up and instrumentations for compression and four-point bending test of VHSC encased composite columns. The compression test (shown in Fig.3(a)) was performed in a 10 MN testing actuator operated in displacement-control mode. One of two special designed solid pin-pin supports was set on the rigid column base, while the other one was bolted to the actuator. The supports included a cylinder that simulated a line load on the specimens, which allowed rotation. The specimens were set into the supports through the bolt connection. According to the previous literatures (Kim *et al*. 2012, Huang and Liew 2016b, Du *et al*. 2017), the boundary conditions of the columns were pin-pin supported. For bending test, the composite column experienced a monotonic four-point bend

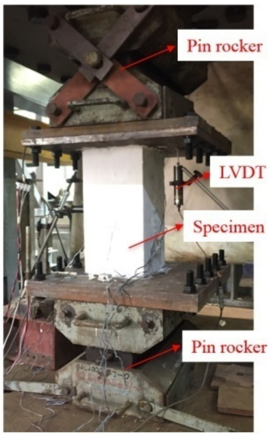

(a) Compression

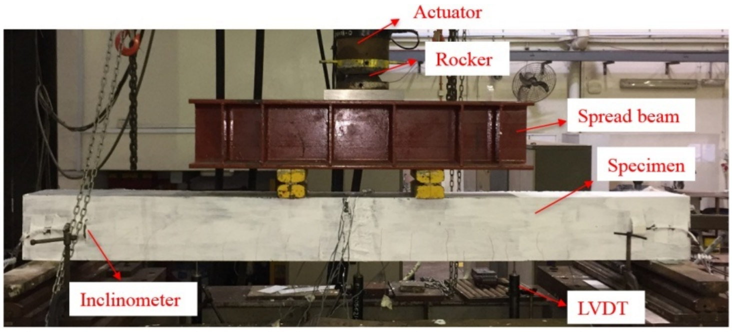

(b) Pure bending

Fig. 3 Test setup for composite columns

loading, performed in a 1,000 kN universal testing machine operated in a displacement-controlled mode. The composite column had a clear span of 1800 mm. The specimen experienced pure bending in the central span of 500 mm between the two loading points, applied by a spread beam placed on the composite beam, as shown in Fig. 3(b).

Each specimen was instrumented with steel strain gauges, linear variable displacement transducers (LVDT), as sketched in Figs. 2 and 3. For short column specimen, on each steel plate, two steel strain gauges (S-steelW and S-steelF) were placed along the longitudinal centerline of the web and flange. Two additional steel strain gauges (S-rebarT and S-rebarC) were placed on the longitudinal bar on both the tension and compression sides. One steel strain gauge (S-shear) was placed on the shear link to measure if there was any early yielding before failure. Four concrete strain gauges (S-conF, S-conB, S-conL and S-conR) were placed on four surfaces. Along the minor axis, two LVDTs were placed vertically to assess axial shortening on compression side and lengthening of specimen on tension side, as shown in Fig. 3. The last LVDT was used to measure the horizontal displacement of the column due to bending. For long column, the steel strain gauges layout was similar to the short column, while the concrete strain gauges differed. Three concrete strain gauges (S-conback1~3) were placed on the longitudinal centerline of the tension face at equal spacing to assess the strain distribution horizontally, and five additional concrete strain gauges (S-conside1~5) were placed along the transverse middle, also at equal spacing (50 mm), to assess the strain distribution of the cross section of the column. Three LVDTs were placed along the longitudinal centerline of the bottom concrete face at equal spacing to measure vertical deflection.

A quasi-static loading procedure is introduced in four steps: (1) preload at a rate of 0.2 mm/min for specimen up to 10% of calculated maximum resistance by Eurocode 4; (2) unload at a rate of 0.5 mm/min for all the specimens; (3) reload at the same rate as in Step 1 until the peak load is reached; (4) finally in the post-peak range, increase the rate to 0.5 mm/min until significant visible deformation is observed.

Table 7 Failure loads and failure modes of specimens

Specimen	P (kN)	M (kN.m)	Primary failure	Other failure
C50e0	3744.1	-	Concrete crushing	Local buckling of rebar
C100e0	6913.4	-	Concrete spalling	Local buckling of rebar
C100e50	3686.7	242.8	Concrete spalling	Local buckling of rebar
C100e105	1800.5	209.7	Tension failure	Concrete crushing
C100B	313.95	149.1	Flexural failure	Slippage of concrete
C100F	7256.9	-	Concrete splitting	Concrete crushing

* Primary failure governs the failure procedure of specimens; other failure is side effect of failure procedure of specimens

3. Test results

3.1 Failure modes

All the specimens were tested to failure. Table 7 lists the failure loads and summarizes failure modes of the specimens. From the test results, specimen C50e0 under pure compression failed by concrete crushing followed by yielding of reinforcing rebar. The aggregate can be seen intact after concrete spalling, implying that normal concrete was governed by the interfacial transition zone (IZT) failure between aggregates and cement paste (Fig. 4(a)). However, the basic failure of VHSC encased composite column under compression with/without eccentricity was concrete spalling followed by local buckling of rebars, since the spalling concrete lost the bond resistance to the rebar and the shear stirrups. The structural stiffness degraded significantly. Thus, the outer load was transferred to the steel plates and reinforced rebars, causing rebar buckling as shown in Fig. 4(c). The cracking noise was audible while the load approached to the failure load and explosive sound

(a) C50e0 (b) C100F (c) C100e0 (d) C100e50 (e) C100e105

(f) C100B

Fig. 4 Failure modes of test specimens

was heard at failure for C100e0. Visible cracks were observed on the concrete exposed to the surface as approaching to the failure loads. The spalling concrete fragments splashed to the surrounding. The brittle failure mode (C100e0, C100e50) indicated that the strength of steel plate was not fully mobilized because of earlier failure of concrete without insufficient confinement by stirrups. The failure surface of concrete was smooth after removal of the concrete cover, showing the typical concrete aggregate failure. As the loading eccentricity increased (e.g., C100e105), the curvature of the specimen became more pronounced compared with that of other specimens while reaching the ultimate load. The failure was governed by the tensile yielding of reinforced rebar (C100e105). For the specimen under pure bending (C100B), the failure turned into interfacial slippage between the steel and concrete followed by the yielding of the bottom steel plate shown as Fig. 4(f). Vertical flexure cracks appeared within the pure bending region and diagonal shear cracks appeared at shear-span regions under combined shear and bending. The debonding of concrete may give risk to the prefailure of the steel-concrete interface, which weakened the composite action between the steel and concrete, resulting in an unexpected lower moment resistance. For composite column using fiber-reinforced concrete (C100F) with reinforcing rebars removed, the major failure mechanism was combined crushing and splitting of concrete. The inclusion of steel fiber improved the concrete toughness and the bond strength between concrete and steel, which has mobilized the cross-sectional resistance of composite column, though VHSC exhibited splitting mechanism and brittle nature. No severe spalling of concrete was observed during the test, but a major wide crack was generated after failure. Steel fiber was pulled out from the concrete, as shown in Fig. 4(b).

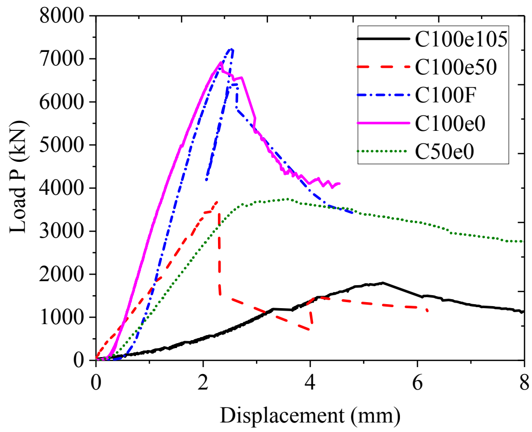

(a) Load-displacement curves of specimens under compression with/without eccentricity

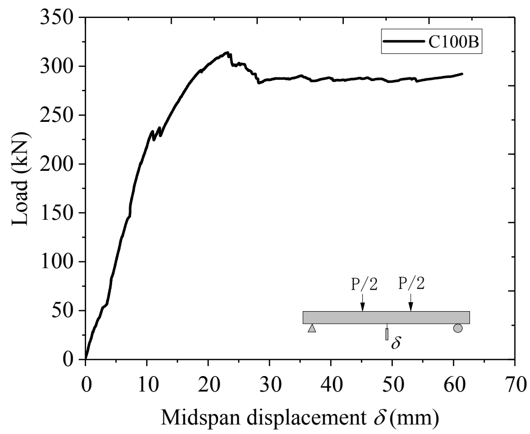

(b) Load-midspan displacement of specimen under four-point bending

Fig. 5 Load-displacement of specimens

3.2 Load-displacement relationship

The load-displacement curves of all specimens are recorded and plotted in Fig. 5. For specimen C50e0 (shown in Fig. 5(a)), the load-displacement curve can be characterized by an upwards trend reaching to the ultimate load followed by a slightly declining trend plateau. For C100e series specimens, the ultimate compressive resistance was significantly larger than that of specimen C50e0, while the descending part after post-yield point was

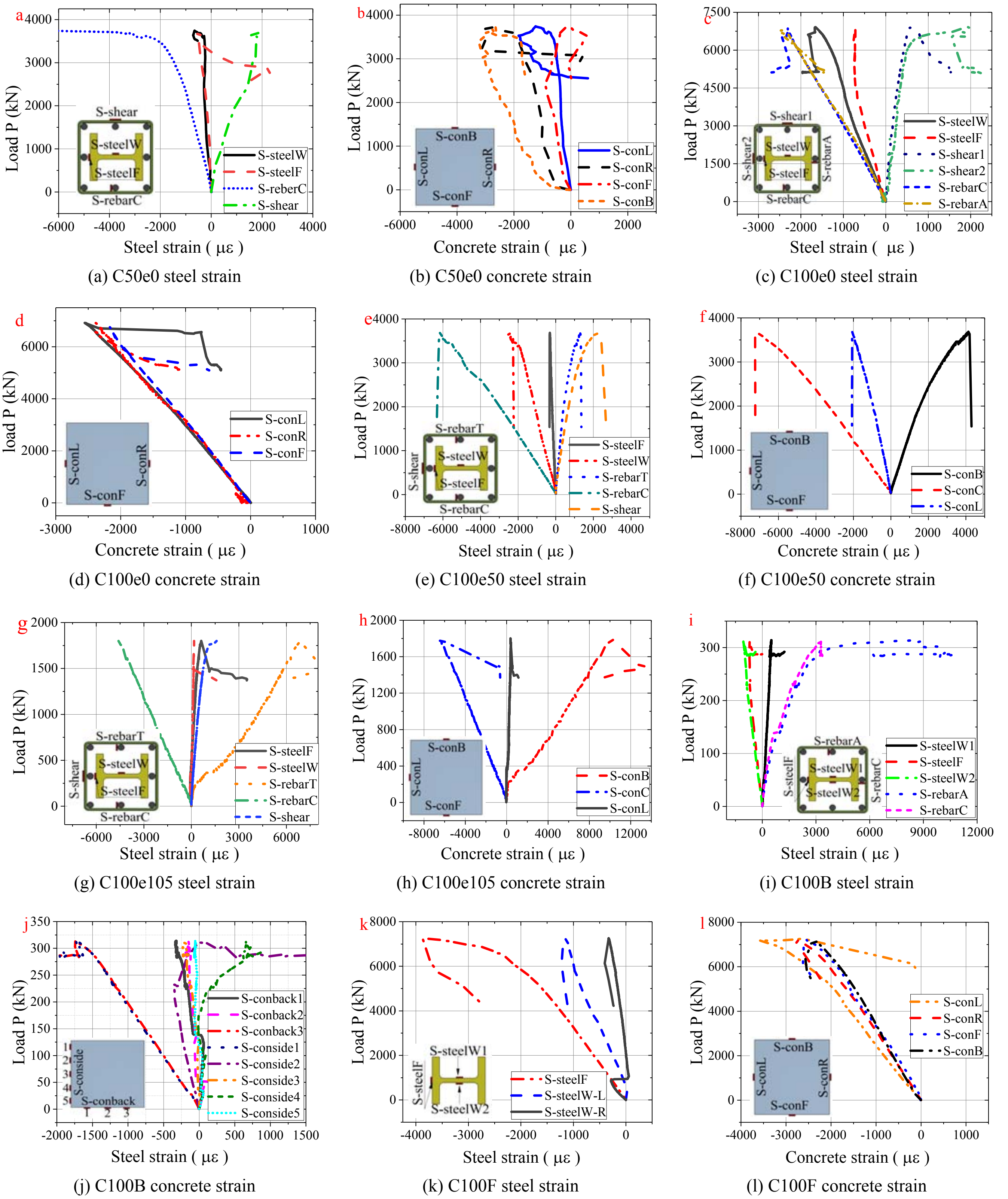

Fig. 6 Load-strain curves for VHSC encased composite column

more brittle than that of specimen C50e0. The secant stiffness of load-shortening curves and the maximum load tended to reduce as the loading eccentricity e increased from 0 to 105 mm. Nevertheless, the ductility of load-shortening curves seemed to be better. For specimen C100F, the ultimate compressive resistance was much larger than that of C50e0. As the loading displacement increased, the load approached to the maximum resistance followed a sudden drop to about two thirds of maximum value, and then regained the load with slightly smaller than the maximum value. The sharp drop resulted from the splitting of fiber reinforced concrete and the fiber were pulled out from the cement paste. The load-displacement curve shows a residual resistance owing to the existent contribution of steel section. Fig. 5(b) shows the load-midspan deflection response of specimen C100B. The first flexural crack appeared in mid-span when the load reached 50 kN, showing the first turning point in the load-deflection curve. The second turning point appeared at approximately 320 kN due to the slippage between concrete and steel, after which the strain increased rapidly as the load decreased. The load-deflection curve exhibited ductile behavior under bending.

3.3 Load-strain relationship

Figs. 6(a)-(l) show the load-strain curves for steel, rebar, shear stirrups and concrete of each specimen. For all the specimens, the shear stirrup had yielded before reaching the failure load of the column, which may result in the prematurely failure of concrete. For specimen series C100e, a distinct sudden drop in load-concrete strain curves was observed as soon as the load was up to the yielding load without a transitional plastic plateau, showing the VHSC exhibited brittleness and explosive nature. However, load-concrete strain curves in C50e0 (Fig. 6(b)) and C100F (Fig. 6(k)) show more ductile behavior which illustrated that the inclusion of steel fiber in concrete may improve the ductility nature of VHSC. The figures in specimen C100e series (Figs. 6(c), (e), (f), (i)) showed that the flange and web of structural steel did not yield at the failure load which indicated that the load carrying capacity of structural steel was not mobilized as a result of the early spalling of weak-confined VHSC and early yielding of shear stirrups. On the contrary, the flange of structural steel yielded before approaching the failure load in C100F, implying that the inclusion of steel fiber can promote the load carrying capacity of structural steel. In addition to specimen C100e50, the rebar in compression zone has yielded before approaching the failure load, while the rebar in the tension zone did not yield, implying that such failure was governed by compression (i.e., compressive yielding of rebar and spalling of concrete). For specimen C100e105, the rebars in tension have yielded before reaching the failure load, while the rebars in compression zone did not yield, implying that such column failure was governed by tension (i.e., tensile yielding of rebars and tensile crack of concrete).

4. Analytical study

4.1 Current code approaches

4.1.1 Eurocode 4 method

To predict the ultimate resistance of composite column under combined compression and uniaxial bending, Eurocode 4 provides a simplified method following the assumptions below: (1) Rectangular plastic stress blocks; (2) Zero concrete tensile strength; and (3) Plane sections remain plane. The N-M interaction formulae are derived for the VHSC encased composite column. The interaction curve can be simplified by a polygonal diagram, depicted by the curve in Fig. 7. The equations describing the polygon points ABCD are elucidated in Part 6.7.3 in Eurocode 4.

4.1.2 ACI 318 method

ACI 318 regards the composite section as an equivalent reinforced concrete section. The calculation method of ACI 318 is based on the strain compatibility method across the whole section. The strain in concrete and non-prestressed reinforcement shall be assumed proportional to the distance from the neutral axis. The design assumptions for concrete are as follows: (a) the maximum strain at extreme concrete compression fiber shall equal to ultimate strain of concrete (e.g., 0.003); (b) the tensile strength of concrete is neglected in flexural and compressive strength calculation; (c) concrete stress distribution was treated as rectangular, trapezoidal, parabolic or other shape agreed with results of comprehensive tests. In this paper, the concrete stress distribution is assumed as rectangular block with a factor α_1 = 0.85 and another factor β_1 are introduced to consider the

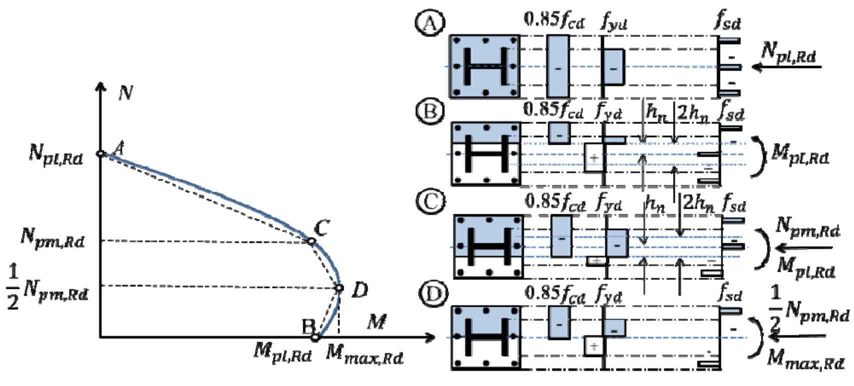

Fig. 7 Simplified N-M interaction model and corresponding stress distribution based on Eurocode 4

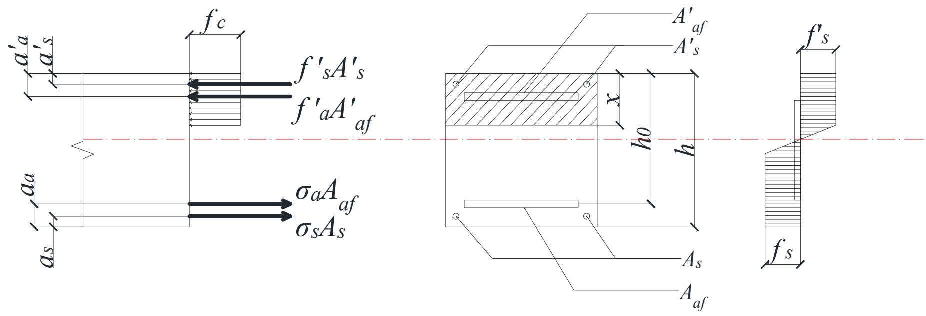

Fig. 8 Calculation model in JGJ 138

reduction of concrete strength and the depth of compression zone, respectively. The factor β_1 refers to Table 22.2.2.4.3 in ACI 318-14.

4.1.3 AISC 360 method (Method I)

The Method I in AISC 360-10 is applicable to doubly symmetric composite beam-columns which are the most common geometry utilized in building construction. The relationship of compression-bending moment (*N-M*) I can be simplified as bilinear interaction curve which only considers two points to define the curve (one for pure bending (point B), and the other for pure compression (point A)). The bilinear interaction curve is defined in Chapter H1.1 in AISC 360.

4.1.4 JGJ 138 Method

The prediction method in Chinese code JGJ 138-2016 is similar to that in ACI 318-14, where the composite section is regarded as an equivalent reinforced concrete section and strain compatibility assumption is employed for calculation. The assumptions of these two methods are similar except the reduction factors of concrete strength α_1 and the depth of compression zone β_1. The two reduction factors in JGJ 138 (2016) are restricted by concrete strength within the range of C20-C80. In this paper, these two factors are obtained from linear interpolation extended from concrete strength of C20-C80. In this method, the section is divided into two parts, namely the concrete section with reinforced rebar and steel flange, and the steel web section. Fig. 8 shows the calculation model of an eccentric loaded concrete encased composite section. The cross-sectional resistance calculation method can refer to Chapter 6.2.2 in JGJ 138 (2016), as shown in Eq. (1).

$$\begin{cases} N = \alpha_1 f_c bx + f_s^{'} A_s^{'} + f_a^{'} A_{af}^{'} - \sigma_s A_s - \sigma_s A_{af} + N_{aw} \\ M = \alpha_1 f_c bx(h_0 - \dfrac{x}{2}) + f_s^{'} A_s^{'}(h_0 - a_s^{'}) + f_a^{'} A_{af}^{'}(h_0 - a_a^{'}) + M_{aw} \end{cases} \tag{1}$$

4.2 Proposed design methods

Due to the brittle nature of the VHSC, early spalling of concrete cover followed by yielding of stirrups (compression) or slippage of concrete (bending) is observed in the test. Therefore, the plastic design for composite column may not be achieved since the material strength has not been mobilized. Thus, a self-programmed nonlinear N-M interaction model with regard to elastic, elastoplastic and plastic methods is proposed to predict the loading capacity of VHSC encased composite columns. Verification between the test results and the predictions by above-mentioned codes are also performed

4.2.1 Constitutive model

The stress-strain curves of VHSC, steel rebar and H-shaped steel are shown in Fig. 9. Many researchers have attempted to develop constitutive models to describe the stress-strain relationship of VHSC in uniaxial compression with/without confinement (Carreira and Chu 1985, Wee *et al.* 1996, Papanikolaou and Kappos 2007, Lim and Ozbakkaloglu 2014, Lu *et al.* 2016, Wang and Liew 2016, Piscesa *et al.* 2017, Chen and Wu 2016, Javed *et al.* 2017). This paper adopts the concrete model proposed

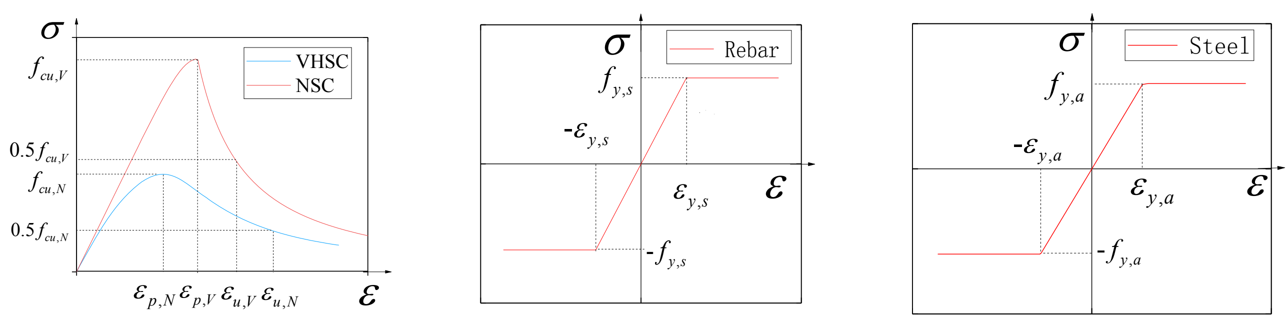

(a) Very high strength concrete and normal strength concrete

(b) Reinforced rebar

(c) Steel

*Subscript: N = Normal Strength Concrete; V = Very High Strength Concrete

Fig. 9 Constitutive models for martials

by Wee *et al*. (1996) that can well represent the strain softening behavior and post-peak behavior of concrete after the peak point. This model is based on the plain concrete in compression proposed by Carreira and Chu (1985). Additional two correction factors (k_1 and k_2 mentioned in Eq. (4)) are applied to describe the post-peak descending branch for high strength concrete. The model shown in Fig. 9(a) consists of ascending and descending branch and is defined according to Eqs. (2-4):

(a) Ascending branch: Eq. (2) represents the relationship between the compressive stress f_c and the compressive strain ε of concrete

$$f_c = f_{cu}\left[\frac{\beta(\varepsilon/\varepsilon_p)}{\beta-1+(\varepsilon/\varepsilon_p)^{\beta}}\right] \tag{2}$$

where $\beta = 0.058f_{cu} + 1.0$ (f_{cu} in MPa), defining the shape of the stress-strain curve. f_{cu}, ε_p are the concrete strength and concrete peak strain respectively. ε_u in Fig. 9(a) is introduced to consider the plastic potential of concrete, defined as the compressive strain corresponding to 50% of the peak strength in the descending branch as proposed by Kim *et al*. (2012).

(b) Descending branch: Eq. (3) represents the relationship between the concrete stress f_c and strain ε of descending branch

$$f_c = f_{cu}\left[\frac{k_1\beta(\varepsilon/\varepsilon_p)}{k_1\beta-1+(\varepsilon/\varepsilon_p)^{k_2\beta}}\right] \tag{3}$$

where the two factors k_1 and k_2 are defined by Wee *et al*. (1996) based on their experimental study on high strength concrete of 50-120 MPa, which are determined by

$$\begin{aligned} k_1 &= (50/f_{cu})^{3.0} \\ k_2 &= (50/f_{cu})^{1.3} \end{aligned} \tag{4}$$

Perfect elastic-plastic model (shown in Fig. 9(b) and (c)) is employed for reinforced rebar and structural steel, calculated by Eqs. (5) and (6), respectively

$$\sigma_s = \begin{cases} E_s\varepsilon, & 0 \le \varepsilon < \varepsilon_{y,s} \\ f_{y,s}, & \varepsilon \ge \varepsilon_{y,s} \end{cases} \tag{5}$$

$$\sigma_a = \begin{cases} E_a\varepsilon, & 0 \le \varepsilon < \varepsilon_{y,a} \\ f_{y,a}, & \varepsilon \ge \varepsilon_{y,a} \end{cases} \tag{6}$$

Where E_s and E_a are the elastic modulus of rebar and steel, respectively; $f_{y,s}$ and $f_{y,a}$ are the yield strength of rebar and steel respectively, while $\varepsilon_{y,s}$ and $\varepsilon_{y,a}$ are the yield strain of rebar and steel, respectively.

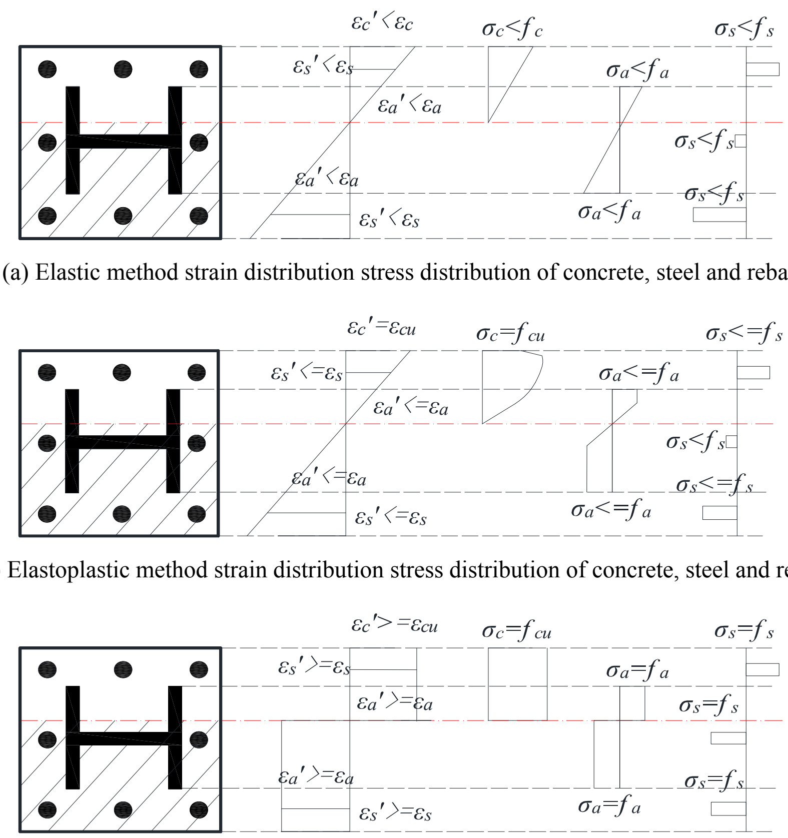

(a) Elastic method strain distribution stress distribution of concrete, steel and rebar

(b) Elastoplastic method strain distribution stress distribution of concrete, steel and rebar

(c) Plastic method strain distribution stress distribution of concrete, steel and rebar

Fig. 10 Strain and stress state in composite section

4.2.2 Assumptions and failure characterization

To simplify the calculation and ensure the accuracy of the predictions, the following assumptions are adopted: (a) plane sections remain plane; (b) zero concrete tensile strength; and (c) strain-compatibility condition. Three typical ultimate limit state design (ULSD) methods are taken into consideration as the failure criterion: (a) elastic method; (b) elastoplastic method; and (c) plastic method, which are shown in Figs. 10(a)-(c) respectively.

(a) Elastic method

For elastic method, the stress state of all the materials is limited within the elastic stage, neglecting their plastic potential. The stress of different materials exhibits a linear distribution across the section. For this ultimate limit state, the materials are considered as elastic-brittle materials where once the material element reaches the yielding point, the element fails and no longer undertakes the stress, losing the stiffness and results in the failure of column section. The brittleness of concrete usually is the trigger of such failure since the peak strain of VHSC is the smallest among the peak stains of different materials.

(b) Elastoplastic method

Elastoplastic method mainly considers the actual stress state of different materials, especially for the high strength concrete. The stress distribution of different materials is determined by the strain compatibility and its stress-strain curves are shown in Fig. 10(b). In this ultimate limit state, the stress of concrete is mainly limited by the ultimate strain ε_u and exhibits nonlinear distribution across the section. The stress state of rebar and steel section can reach their plastic strain depending on the strain evolution.

(c) Plastic method

Plastic method assumes all the materials can fulfill their plastic potential, shown as Fig. 10(c). In such ultimate limit state, the stress distribution diagram of different materials is treated as rectangular blocks, where each element has reached its yield strain. The design methodology for composite column in Eurocode 4 (2004) is based on the plastic method.

4.2.3 Fiber element analysis

The fiber-element model provides a versatile approach for composite design. To simplify the calculation procedure, a self-programmed numerical routine using fiber-element method was adopted to calculate the compressive and bending moment resistance. (Kim *et al.* 2012, Tokgoz *et al.* 2012, Begum *et al.* 2013). Fig. 11 shows the fiber-element model where the section is divided into finite number of elements. The following assumptions are used in the fiber-element analysis:

- Plane sections of the concrete remain plane after bending;
- Creep and shrinkage of concrete is neglected;
- Residual stresses in steel are neglected;
- Tensile strength and tension stiffening of concrete are neglected;
- Shear deformations and torsion are neglected. The integration equations are shown in Eq. (7).

$$\begin{aligned} N &= \sum A_c\sigma_c + \sum A_y\sigma_y + \sum A_s\sigma_s \\ M &= \sum A_c\sigma_c y_c + \sum A_y\sigma_y y_y + \sum A_s\sigma_s y_s \end{aligned} \tag{7}$$

where A_c, A_y, and A_s, are the fiber element area of the concrete, steel and reinforced rebar, respectively; σ_c, σ_y and σ_s are the stress of concrete, steel and reinforced rebar, respectively, which can be calculate by $\sigma_x = E_x\varepsilon$; y_c, y_y and y_s are distance from the fiber of concrete, steel and reinforced rebar to the neutral axis, respectively.

This paper proposed an efficient image-oriented intelligent recognition subroutine incorporated in the fiber-element analysis to improve the calculation accuracy. Each material element is pixilated through RGB color value stored as a three-dimensional area-matrix. The accuracy of analysis depends on the image resolution. By converting the three-dimensional area-matrix into the two-dimensional matrix, the section is transferred into digital elements automatically while the material matrix showing the distribution of material area is determined based on the RGB value. Fig. 12(a) shows a typical pixilated image of column section. To obtain the ultimate resistance (including the compressive and moment resistance) of composite column subjected to eccentric load, two equilibrium equations shown in Eq. (1) are derived. Given the neutral axis distance x_c, the strain vector ε_i along the section depth can be determined based on the plane section remain plane assumption. Then the strain matrix $\varepsilon_{i,j}$ showing the strain distribution of the whole section is generated according to strain-compatibility condition. The stress $\sigma_{i,j}$ of each fiber element in the section can be determined based on the constitutive models. Figs. 12(b) and (c) show the strain and stress distribution of the section within the elastic limit state with the neutral axis located at the center of the section. Hence, each point in the N-M curve representing the axial

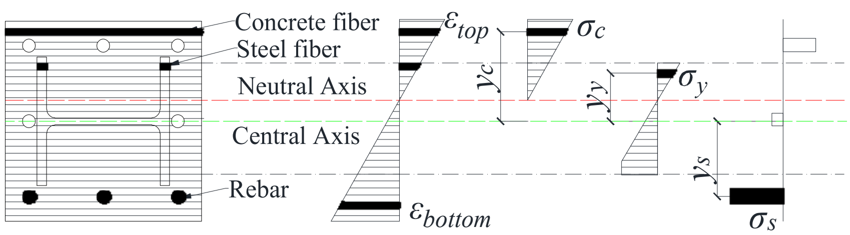

*Fiber section strain distribution, stress distribution of concrete, steel and rebar

Fig. 11 Fiber element method

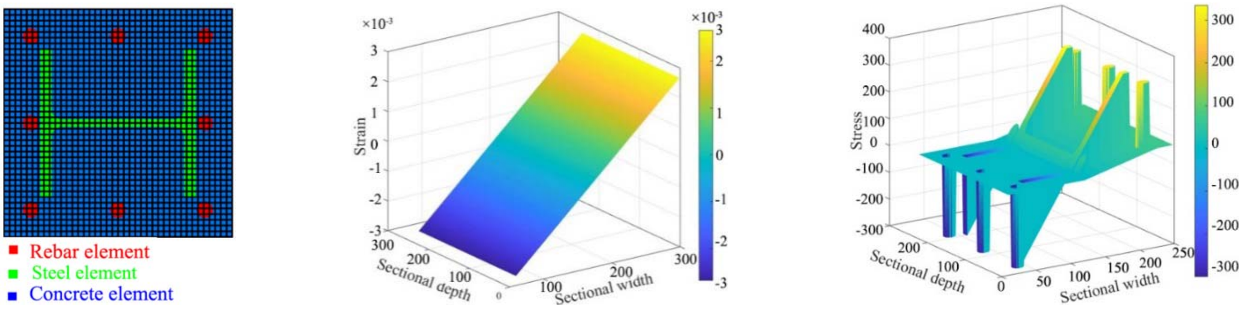

(a) Element section (b) Strain distribution (c) Stress distribution

Fig. 12 Image-oriented based fiber element analysis

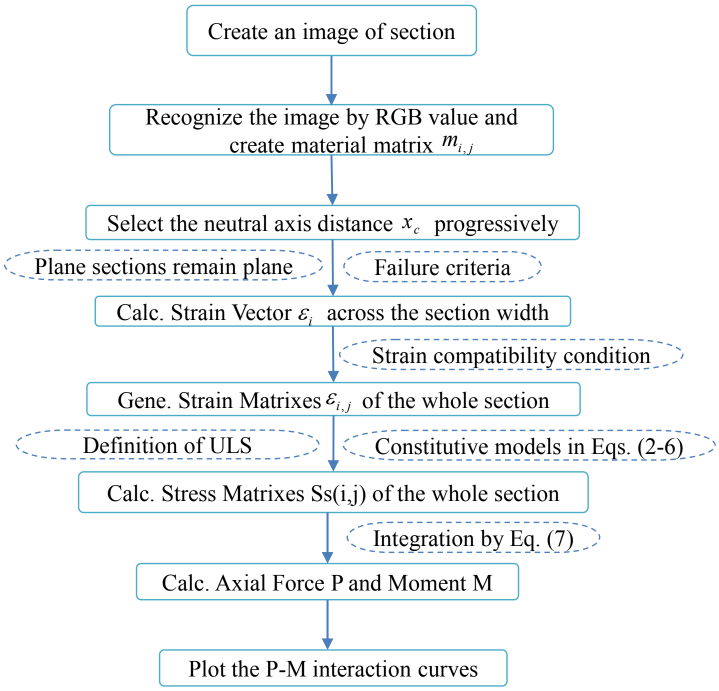

Fig. 13 Flow diagram

force and end moment can be determined through integration of stress across the section depth. A subroutine is programmed using MATLAB to calculate the load resistance of composite column. Fig. 13 illustrates the main flow diagram of the program. Fig. 14 shows the output relationship curve of axial force and end moment of elastoplastic method, where the stress distribution conditions of four characteristic points are displayed.

4.3 Verification

All the partial factors are taken as 1.0 (safety factor ψ in JGJ 138-2016, resistance factor φ in LRFD design and safety factor Ω for ASD design in AISC 360-10) for comparison with test results. Fig. 15 and Table 8 show the test results and predictions of current codes as well as the proposed three methods. The slenderness of specimens is out of consideration as all the specimens are short stub columns. Eurocode 4 and JGJ 138 that utilize the plastic analysis over-predict the resistance of the VHSC encased column, especially for eccentric loaded composite columns

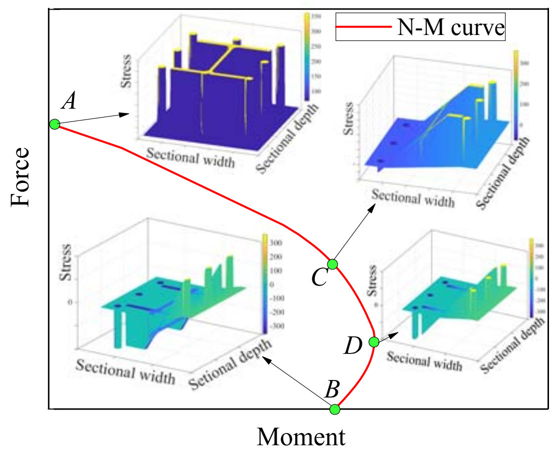

Fig. 14 Representative points in N-M interaction model using elastoplastic method

with larger loading eccentricity. Method I in AISC 360 is overconservative in the prediction of compression with

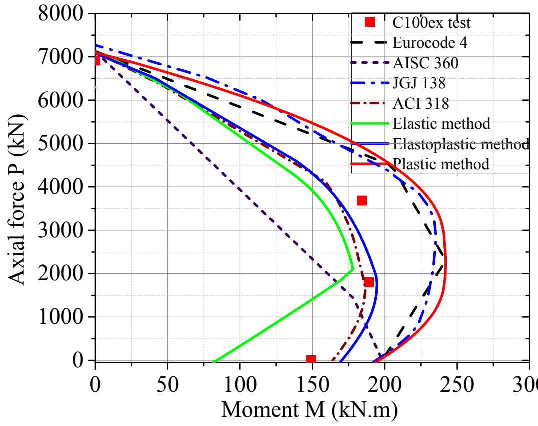

Fig. 15 Comparisons among test results, code predictions and predictions by the proposed methods

small eccentricity, e.g., 25.2% smaller than the test result of C100e50. ACI 318 method that utilizes the strain-compatibility assumption well-predicts the eccentric compressive resistance. The prediction curve of ACI 318 keeps closely identical with that of elastoplastic method. From Fig. 15, the elastoplastic design method gives close predictions compared with the test results. However, it is found that all the methods except the elastic method predict higher than the result of the pure bending test, with the test point falling within the N-M interaction curve. It is due to the failure of flexural specimen prematurely initiated by debonding of concrete and steel which leads to lower composite action of the composite section. The principles of plane sections remain plane and the strain-compatibility condition in this case is no more satisfied. This suggests that in the case of pure bending or loading with larger eccentricity, full composite design with sufficient shear connections for VHSC encased composite member is recommended.

To further verify the applicability of numerical procedure, a database (Ye 1995, Lou 1996, Gentian *et al.* 2006, Wang 2007, Zhang 2011, Kim *et al.* 2012, 2014, Begum *et al.* 2013) of concrete encased composite column subjected to eccentric compression loads is collected in Table 9. The proposed three methods are applied to be verified by the test data. Fig. 16(a) shows the comparison between the test results and the predictions of the proposed methods. The solid points represented the test data in this paper, while the hollow points are test data collected from the literature. The elastic method gives very conservative predictions compared with that of the test results. It is because the elastic resistance is defined based on the first cracking load. The elastoplastic method provides close predictions while the plastic method gives unconservative predictions, with the mean value P_{ep}/P_t and P_p/P_t of 0.88 and 1.14, respectively. To better understand the influence of concrete strength on the behaviour of VHSC encased composite column, the database is divided into two groups with the range of concrete strength from 20 to 60 MPa and 60 to 120 MPa, respectively, which is shown as Figs. 16(b) and (c). The plastic method gives close predictions of the load resistance of composite column using normal concrete strength from 20 to 60 MPa, with the mean value P_p/P_t of 0.94 and the standard deviation of 0.12. However, the mean value of P_p/P_t is 1.37 and the standard deviation is 0.34 for the composite column using high strength concrete from 60 to 120 MPa. This indicates that the plastic method may not be applicable for the prediction of ultimate resistance of composite column using high strength concrete. Nevertheless, the elastoplastic method gives closer predictions with the mean value P_{ep}/P_p of 1.02 and the standard deviation of 0.13 for composite column using high strength concrete from 60 to 120MPa which implies that the elastoplastic method serves as a more reasonably accurate and design method.

5. Conclusions

This paper presents experimental and analytical investigation on the structural behavior of very high strength concrete (VHSC) encased steel composite columns subjected to axial compression and end moment. A series of combined compression and uni-axial bending tests on VHSC concrete encased composite columns have been carried out. A reasonable elastic-plastic method using fiber element method is developed. The following conclusions are derived based on the experimental and analytical investigations:

(1) The VHSC concrete encased composite columns exhibits brittle and explosive spalling failure mode under axial compression. Early spalling may be due

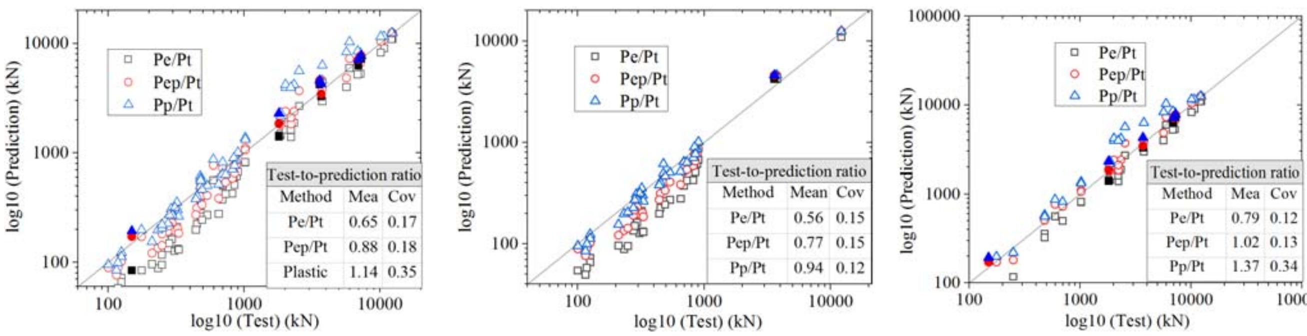

(a) Concrete strength 20-120 MPa (b) Concrete strength 20-60 MPa (c) Concrete strength 60-120 MPa

Fig. 16 Comparison between the test results and prediction to the insufficient confined stirrups based on current design guides. The major failure mode observed from the tests is splitting of high strength concrete followed by local buckling of longitudinal reinforcement.

(2) A novel steel fiber reinforced concrete encased composite column without any rebars or stirrups has been proposed for application. The test result shows that steel fiber improves the crack resistance of high strength concrete, but the major failure of such composite column under compression is still brittle due to direct crack propagation without confinement effect provided by the shear stirrups. Compared to rebar reinforced concrete encased composite column using normal concrete, longitudinal rebar offers softened unloading behavior. However, the novel section is able to achieve the cross-sectional resistance which indicates the rebar reinforcement can be reduced or even removed such that it eliminates the tedious detailing works and therefore spurs the construction, improves the productivity in fabrication and eases the installation of beam-column joints.

(3) For pure compression and eccentric compression with small load eccentricity, cross-sectional plastic resistance can be achieved while for pure bending and eccentric compression with large load eccentricity, sectional plastic resistance cannot be achieved. From this point of view, the plastic design approach for composite columns in current codes may not be directly applied to predict the loading resistance of VHSC encased composite column subjected to combined compression and end moment. An image-oriented intelligent-recognition based elastic-plastic method using fibre element analysis is employed to predict the combined resistance of the composite column. The validation against the test data shows that reasonable and conservative predictions could be achieved compared to that using current code methods. For design purpose, Eqs. (1-6) are recommended to predict the design resistance of the VHSC encased composite columns having proper consideration of the material partial factors.

(4) A database related to the high strength concrete encased composite column under eccentric loads is collected to verify the proposed elastic, elastoplastic and plastic method. It turns out that the plastic method can give close predictions of the load resistance in composite column using normal concrete strength (20-60 MPa) while the elastoplastic method can give closer predictions in the case of high concrete strength (60-120 MPa).

This study investigates the structural behavior of VHSC encased composite column experimentally by limiting parameters. Further study should extend to investigate a wider range of parameters, e.g., provide closer shear stirrups to confine the high strength concrete core, steel fiber content and type. Development of novel shear links could also be helpful to achieve stain compatibility between very high strength concrete and high strength steel.

Acknowledgments

The authors would like to acknowledge the research grant received from the National Natural Science Foundation of China (NSFC, No. 51708360, 51678365), Ministry of Education (MOE) in Guangdong Province (No. 2017KTSCX164), Scientific Research Startup Fund of Shenzhen University (No. 2018023) and the Postgraduate Innovation Development Fund Project of Shenzhen University (No. 00004133).

References

ACI 318 (2014), Building Code Requirements for Structural Concrete; American Concrete Institude, Farmington Hills, MI48331, USA.

AIJ (2010), Standard for Structural Calculation of Steel Reinforced Concrete Structures; Architectural Institute of Japan, Tokyo, Japan.

AISC 360 (2010), Specification for Structural Steel Buildings; Chicago, IL, USA

ASTM C39/C39M (2014), Standard Test Method for Compressive Strength of Cylindrical Concrete Specimens; West Conshohocken, PA, USA.

ASTM C136/C136M – 14 (2014), Standard Test Method for Sieve Analysis of Fine and Coarse ;ggregates, West Conshohocken, PA, USA.

ASTM C1611/C1611M-14(2018), Standard test method for slump flow of self-consolidating concrete; West Conshohocken, PA, USA.

ASTM E8/E8M - 16A (2016), Standard Test Methods for Tension Testing of Metallic Materials; West Conshohocken, PA, USA.

Bărbos, G.A. (2016), "Long-term Behavior of Ultra – High Performance Concrete (UHPC) Bended Beams", *Procedia Technology*, **22**(1), 203-210.

Begum, M., Driver, R.G. and Elwi, A.E. (2013), "Behaviour of partially encased composite columns with high strength concrete", *Eng. Struct.*, **56**(1), 1718-1727.

Carreira, D.J. and Chu, K.H. (1985), "Stress-strain relationship for plain concrete in compression", *ACI Journal*, **82**(6), 797-804.

Chen, S. and Wu, P. (2016), "Analytical model for predicting axial compressive behavior of steel reinforced concrete column", *J. Const. Steel Res.*, **128**, 649-660.

Choe, G., Kim, G., Gucunski, N. and Lee, S. (2015), "Evaluation of the mechanical properties of 200MPa ultra-high-strength concrete at elevated temperatures and residual strength of column", *Constr. Build. Mater.*, **86**(1), 159-168.

Deng, Z. and Qu, J. (2015), "The experimental studies on behavior of ultrahigh-performance concrete confined by hybrid fiber-reinforced polymer tubes", *Adv. Mater. Sci. Eng.*, 1-18.

Du, Y., Chen, Z., Wang, Y.-B. and Richard Liew, J.Y. (2017), "Ultimate resistance behavior of rectangular concrete-filled tubular beam-columns made of high-strength steel", *J. Const. Steel Res.*, **133**, 418-433.

El-Tawil, S. and Deierlein, G.G. (1999), "Strength and ductility of concrete encased composite columns", *J. Struct. Eng.*, **125**(9), 1009-1019.

Ellobody, E. and Young, B. (2011), "Numerical simulation of concrete encased steel composite columns", *J. Const. Steel Res.*, **67**(2), 211-222.

Ellobody, E., Young, B. and Lam, D. (2011), "Eccentrically loaded concrete encased steel composite columns", *Thin-Wall. Struct.*, **49**(1), 53-65.

Elwi, A.E., Begum, M. and Driver, R.G.(2015), "Parametric study on eccentrically-loaded partially encased composite columns under major axis bending", *Steel Compos. Struct., Int. J.*, **19**(5), 1299-1319.

Eurocode 2 (2004), Design of concrete strctures, part 1-1: General rules and rules for buildings; European Committee for Standardisation, Brussels, Belgium.

Eurocode 4 (2004), EN 1994-1-1 Design of composite steel and concrete structures; European Committee for Standardisation, Brussels, Belgium.

Gentian, Z., Chunhua, W., Chunyan, G. and Chenxia, W. (2006), "Experimental study on Mechanical behavior of long columns under eccentric Compression of Steel reinforced concrete", *J. Baotou Univ. Iron Steel Technol.*, **25**(4), 384-400.

Huang, Z. and Liew, J.Y.R. (2016a), "Structural behaviour of steel–concrete–steel sandwich composite wall subjected to compression and end moment", *Thin-Wall. Struct.*, **98,** 592-606.

Huang, Z. and Liew, J.Y.R. (2016b), "Steel-concrete-steel sandwich composite structures subjected to extreme loads", *Int. J. Steel Struct.*, **16**(14),1009-1028.

Huang, Z.Y., Wang, J.Y., Liew, J.R. and Marshall, P.W. (2015), "Lightweight steel-concrete-steel sandwich shell subject to punching shear", *Ocean Eng.*, **102**, 146-161.

Javed, M.F., Sulong, N.H.R., Memon, S.A., Rehman, S.K.U. and Khan, N.B. (2017), "FE modelling of the flexural behaviour of square and rectangular steel tubes filled with normal and high strength concrete", *Thin-Wall. Struct.*, **119**, 470-481.

JGJ 138 (2016), Code for design of composite structure, Ministry of Housing and Urban-Rural Construction of the People's Republic of China; Beijing, China

Kim, C.S., Park, H.G., Chung, K.S. and Choi, I.R. (2012), "Eccentric Axial Load Testing for Concrete-Encased Steel Columns Using 800 MPa Steel and 100 MPa Concrete", *J. Struct. Eng.*, **138**(8), 1019-1031.

Kim, C.S., Park, H.G., Chung, K.S. and Choi, I.R. (2014), "Eccentric axial load capacity of high-strength steel-concrete composite columns of various sectional shapes", *J. Struct. Eng.*, **140**(4), 04013091.

Kim, C.S., Park, H.G., Choi, I.R. and Chung, K.S. (2017a), "Effect of Sustained Load on Ultimate Strength of High-Strength Composite Columns Using 800-MPa Steel and 100-MPa Concrete", *J. Struct. Eng.*, **143**(3), 04016189.

Kim, C.S., Park, H.G., Lee, H.J., Choi, I.R. and Chung, K.S. (2017b), "Eccentric axial load test for high-strength composite columns of various sectional configurations", *J. Struct. Eng.*, **43**(8), 04017075.

Lee, J.H. (2013), "Evaluation on Fire Resistance of Ultra-High-Strength Concrete Depending on Aggregates and Fibers Types", *J. Kor. Soc. Hazard Mitigat.*, **13**(6), 91-97.

Lim, J.C. and Ozbakkaloglu, T. (2014), "Stress–strain model for normal- and light-weight concretes under uniaxial and triaxial compression", *Constr. Build. Mater.*, **71**, 492-509.

Lin, M. (2006), *Study on High Strength Steel Reinforced Concrete Columns*, Xi'an University of Architectural Science and Technology, Xi'an, China.

Lou, Y. (1996), "Simplified calculation method for stiffened concrete long columns", *Indust. Constr.*, **26**(3), 20-22.

Lu, X.L., Yin, X.W. and Jiang, H.J. (2014), "Experimental study on hysteretic properties of SRC columns with high steel ratio", *Steel Compos. Struct., Int. J.*, **17**(3), 287-303.

Lu, D., Du, X., Wang, G., Zhou, A. and Li, A. (2016), "A three-dimensional elastoplastic constitutive model for concrete", *Comput. Struct.*, **163**, 41-55.

Papanikolaou, V.K. and Kappos, A.J. (2007), "Confinement-sensitive plasticity constitutive model for concrete in triaxial compression", *Int. J. Solids Struct.*, **44**(21), 7021-7048.

Pereira, M.F., Nardin, S.D. and Debs, A.L.H.C.E. (2016), "Structural behavior of partially encased composite columns under axial loads", *Steel Compos. Struct., Int. J.*, **20**(6), 1305-1322.

Piscesa, B., Attard, M.M., Samani, A.K. and Tangaramvong, S. (2017), "Plasticity Constitutive Model for Stress-Strain Relationship of Confined Concrete", *ACI Struct J.*, **114**(2), 361-371.

Tokgoz, S., Dundar, C. and Tanrikulu, A.K. (2012), "Experimental behaviour of steel fiber high strength reinforced concrete and composite columns", *J. Const. Steel Res.*, **74**(1), 98-107.

Wang, Z. (2007), *Experimental Study and Nonlinear Analysis of Eccentric Columns with High Strength and High Performance of Steel Reinforced Concrete*, Xi'an University of Architectural Science and Technology, Xi'an, China.

Wang, Y.B. and Liew, J.Y.R. (2016), "Constitutive model for confined ultra-high strength concrete in steel tube", *Constr. Build. Mater.*, **126**, 812-822.

Wee, T.H., Chin, M.S. and Mansur, M.A. (1996), "Sress-strain relationship of high-strength concrete in compression", *J. Mater. Civil Eng.*, **8**(2), 70-76.

Xiong, M. and Liew, J.Y.R. (2016), "Mechanical behaviour of ultra-high strength concrete at elevated temperatures and fire resistance of ultra-high strength concrete filled steel tubes", *Mater. Des.*, **104**(1), 414-427.

Yang, Y., Chen, Y., Zhang, J., Xue, Y., Liu, R. and Yu, Y. (2018), "Experimental investigation on shear capacity of partially prefabricated steel reinforced concrete columns", *Steel Compos. Struct., Int. J.*, **28**(1), 73-82.

YB 9082 (2007), Technical specification for steel reinforced concrete structures; General Institute of Architectural Research of China Metallurgical Group, Beijing, China.

Ye, L. (1995), "Experimental study on stiffened reinforced concrete columns under eccentric compression", *J. Architect. Struct.*, **16**(6), 45-52.

Zhang, L. (2011), *Theoretical Study on the Mechanical Behavior and Design Calculation of High Strength and High Performance Concrete Columns with Steel Profile*, Xi'an University of Architectural Science and Technology, Xi'an, China.

Zhu, W., Jia, J. and Zhang, J. (2017), "Experimental research on seismic behavior of steel reinforced high-strength concrete short columns", *Steel Compos. Struct., Int. J.*, **25**(5), 603-615.

Zohrevand, P. and Mirmiran, A. (2013), "Stress-Strain Model of Ultrahigh Performance Concrete Confined by Fiber-Reinforced Polymers", *J. Mater. Civil Eng.*, **25**(12), 1822-1829.

CC